The Physical Spectrum of a Driven Jaynes-Cummings Model

L. Medina-Dozal , A.R. Urzua , I. Ramos-Prieto , R. Roman-Ancheyta , F. Soto-Eguibar , H.M. Moya-Cessa * , J. Récamier

Posted Date: 24 December 2025

doi: 10.20944/preprints202512.2252.v1

Keywords: driven Jaynes-Cummings model; dynamic physical spectrum; invariant approach; two-time correlations functions; Eberly-Wodkiewicz spectrum

Article

The Physical Spectrum of a Driven Jaynes-Cummings Model

L. Medina-Dozal [1], A.R. Urzúa [1], I. Ramos-Prieto [2], R. Román-Ancheyta [3], F. Soto-Eguibar [2], H.M. Moya-Cessa [2,*] and J. Récamier [1]

[1] Instituto de Ciencias Físicas, Universidad Nacional Autónoma de México, Avenida Universidad s/n, Col. Chamilpa, Cuernavaca, Morelos, 62210 Mexico
[2] Instituto Nacional de Astrofísica Óptica y Electrónica, Calle Luis Enrique Erro No. 1, Santa María Tonantzintla, Puebla 72840, Mexico
[3] Centro de Física Aplicada y Tecnología Avanzada, Universidad Nacional Autónoma de México, Boulevard Juriquilla 3001, Querétaro 76230, Mexico
* Correspondence: hmmc@inaoep.mx

Abstract

We investigate the time-dependent physical spectrum of the driven Jaynes-Cummings model, where both the atom and the quantized field are simultaneously driven by an external classical field. By leveraging the mapping of the time-dependent Hamiltonian onto the standard stationary Jaynes-Cummings form via unitary transformations, we determine the exact two-time correlation functions for both the atomic and field subsystems. These are then employed to compute the time-dependent physical spectrum using the Eberly-Wódkiewicz formalism. Our results demonstrate that the atomic spectral features are significantly reshaped by the external driving, exhibiting tunable asymmetries and shifts. Notably, we find that the driving parameters can be tuned to exactly cancel the initial coherent field amplitude, leading to an effective vacuum limit that recovers the fundamental vacuum Rabi splitting. This provides a clear interpretation of the emission dynamics in terms of the coherent displacement of the cavity field induced by the external drive.

Keywords: driven Jaynes-Cummings model; dynamic physical spectrum; invariant approach; two-time correlations functions; Eberly-Wodkiewicz spectrum

1. Introduction

The Jaynes-Cummings model remains a cornerstone of quantum optics, providing a fundamental and mathematically rigorous description of light-matter interactions at the single-quantum level [1,2]. Since its conceptual formulation, the model has been experimentally validated across diverse physical platforms, most notably in the strong-coupling regime of circuit quantum electrodynamics [3,4]. By modeling the interaction between a two-level system and a single quantized electromagnetic mode, the Jaynes-Cummings model has served as an ideal paradigm for investigating quintessential non-classical phenomena, including the periodic collapse and revival of atomic inversion [5], vacuum Rabi splitting [6–9], and the generation of Schrödinger cat states [10]. Over the decades, the framework has been extended to accommodate dissipation and decoherence in lossy cavities [11,12], as well as nonlinear interactions including multi-photon processes and nonlinear coherent states [13–16]. Modern developments have further expanded the reach of the Jaynes-Cummings model, scaling it to many-body systems via circuit quantum electrodynamics lattices for quantum simulation [17], and exploring generalized frameworks such as the anisotropic quantum Rabi model, which allows for the simultaneous treatment of Jaynes-Cummings and anti-Jaynes-Cummings regimes [18]. Recent spectroscopic studies on nonlinear Jaynes-Cummings model variants have also uncovered novel coupling regimes and spectral asymmetries [19]. A particularly versatile generalization is the driven

 doi:10.20944/preprints202512.2252.v1

Jaynes-Cummings model, where external classical fields act on the atom, the cavity mode, or both, enabling control over the system's quantum state [20–22].

Solving the time-dependent Schrödinger equation for systems characterized by non-stationary interactions remains a formidable mathematical task, often requiring perturbative expansions or specialized numerical techniques. However, for the driven Jaynes-Cummings model with simultaneous atomic and field driving, exact analytical solutions have recently been established through a dynamic invariant approach [23]. Rooted in the foundational theory of time-dependent invariants [24], this framework utilizes a sequence of unitary transformations to map the complex time-dependent Hamiltonian onto a solvable stationary form [23]. Within this formalism, the specific unitary transformations not only determine the dynamical invariant but also provide a mechanism to either factorize the Hamiltonian's temporal dependence or eliminate it entirely in a suitable rotating frame, thereby granting rigorous, non-perturbative access to the system's complete quantum state vector [25–27].

On the other hand, while the state vector contains all dynamical information, extracting experimentally accessible observables requires careful consideration of the measurement process, particularly for non-stationary signals where phase-dependent fluctuations play a crucial role [28]. Conventional quantities like atomic inversion or mean photon number provide only partial insights into the energy exchange dynamics and often mask the fine spectral details of transient phenomena. To fully characterize the time-frequency properties of the emission, one must adopt the physical spectrum of light as defined by Eberly and Wódkiewicz [29], which explicitly accounts for the finite bandwidth and response time of the detector [30,31]. This operational approach has been fundamental in elucidating the spectral signatures of vacuum Rabi splitting in standard atom-cavity systems [6–9].

Building upon this analytical and observational foundation, the present study investigates the time-dependent physical spectrum of the fully driven Jaynes-Cummings model. We derive exact expressions for the two-time correlation functions of both the atomic and field subsystems, enabling a precise mapping of the spectral distribution as it evolves in time. Our analysis reveals that the external driving mechanism induces a coherent displacement of the cavity field [23], which acts to fundamentally reshape the vacuum Rabi spectrum; a phenomenon that has also been explored in the context of nonlinear Jaynes-Cummings models [19]. This dynamic restructuring manifests as tunable asymmetries and shifts in the spectral peaks, offering a highly controllable spectroscopic signature of the driven light-matter interaction.

The remainder of this paper is organized as follows. Section 2 outlines the theoretical model and reviews the invariant method used to diagonalize the driven Hamiltonian. In Section 3, we derive the exact expressions for the time-dependent physical spectrum of the atom and the field, highlighting the spectral signatures of the external drive. Finally, Section 4 provides concluding remarks.

2. The Driven Jaynes-Cummings Model

Consider a system composed of a two-level atom, with ground state $|g\rangle$ and excited state $|e\rangle$ and transition frequency ω_{eg}, interacting with a single quantized electromagnetic field mode of frequency ω_c. The system is enclosed within a high-quality cavity and is simultaneously driven by an external classical field of frequency ω_0 that couples to both the atomic and photonic degrees of freedom, as illustrated in Figure 1. Under the dipole and rotating-wave approximations, the time-dependent Hamiltonian in the laboratory frame is given by [20,23]:

$$\begin{aligned}\hat{H}_{\mathtt{DJCM}}(t) = \omega_c\,\hat{a}^\dagger\hat{a} + \frac{\omega_{eg}}{2}\hat{\sigma}_z + g\left(\hat{\sigma}_+\hat{a} + \hat{\sigma}_-\hat{a}^\dagger\right) \\ + \zeta\left(\hat{\sigma}_- e^{\mathrm{i}\omega_0 t} + \hat{\sigma}_+ e^{-\mathrm{i}\omega_0 t}\right) + \xi\left(\hat{a}e^{\mathrm{i}\omega_0 t} + \hat{a}^\dagger e^{-\mathrm{i}\omega_0 t}\right),\end{aligned} \tag{1}$$

where g denotes the atom-cavity coupling strength, while ζ and ξ represent the driving amplitudes for the atom and the field, respectively. The field annihilation and creation operators, $\hat{a}$ and $\hat{a}^\dagger$, satisfy the commutation relation $[\hat{a}, \hat{a}^\dagger] = 1$. The atomic components are described by the pseudo-spin operators

 doi:10.20944/preprints202512.2252.v1

$\hat{\sigma}_z = |e\rangle\langle e| - |g\rangle\langle g|$, $\hat{\sigma}_+ = |e\rangle\langle g|$, and $\hat{\sigma}_- = |g\rangle\langle e|$, which obey the standard commutation relations $[\hat{\sigma}_+, \hat{\sigma}_-] = \hat{\sigma}_z$ and $[\hat{\sigma}_z, \hat{\sigma}_\pm] = \pm 2\hat{\sigma}_\pm$.

Following the invariant-based approach detailed in [23], we first transition to a rotating frame via the time-dependent unitary transformation $\hat{T}(t) = \exp[i\omega_0 t(\hat{a}^\dagger\hat{a} + \hat{\sigma}_z/2)]$. This procedure eliminates the explicit time dependence of the driving terms, yielding the effective Hamiltonian:

$$\begin{aligned}\hat{H}_T &= \hat{T}(t)\hat{H}_{\mathtt{DJCM}}(t)\hat{T}^\dagger(t) - \mathrm{i}\left(\frac{\partial \hat{T}(t)}{\partial t}\right)\hat{T}^\dagger(t) \\ &= \Delta_c\,\hat{a}^\dagger\hat{a} + \frac{\Delta_{eg}}{2}\hat{\sigma}_z + g\left(\hat{\sigma}_+\hat{a} + \hat{\sigma}_-\hat{a}^\dagger\right) + \zeta(\hat{\sigma}_- + \hat{\sigma}_+) + \xi\left(\hat{a} + \hat{a}^\dagger\right),\end{aligned} \tag{2}$$

where $\Delta_c = \omega_c - \omega_0$ and $\Delta_{eg} = \omega_{eg} - \omega_0$ are the cavity and atomic detunings, respectively. To further simplify the dynamics, the linear driving terms can be removed using the displacement operator $\hat{D}(\alpha) = \exp[\alpha(\hat{a}^\dagger - \hat{a})]$ [32]. Under the matching condition $\alpha = \zeta/g = \xi/\Delta_c$, the Hamiltonian maps exactly onto the stationary Jaynes-Cummings form:

$$\hat{H}_D = \hat{D}(\alpha)\hat{H}_T\hat{D}^\dagger(\alpha) = \Delta_c\hat{a}^\dagger\hat{a} + \frac{\Delta_{eg}}{2}\hat{\sigma}_z + g\left(\hat{\sigma}_+\hat{a} + \hat{\sigma}_-\hat{a}^\dagger\right) - \frac{\zeta\xi}{g} = \hat{H}_{\mathtt{JCM}} - \frac{\zeta\xi}{g}. \tag{3}$$

The exact time-evolution operator for the original driven system, $\hat{U}_{\mathtt{DJCM}}(t)$, is then synthesized by reversing the transformation sequence:

$$\hat{U}_{\mathtt{DJCM}}(t) = \hat{T}^\dagger(t)\hat{D}^\dagger(\alpha)\hat{U}_{\mathtt{JCM}}(t)\hat{D}(\alpha), \quad \hat{U}_{\mathtt{JCM}}(t) = e^{-\mathrm{i}\hat{H}_{\mathtt{JCM}}t}. \tag{4}$$

The residual term $-\zeta\xi/g$ in Eq. (3) introduces only a global phase to the state vector, representing a constant energy shift that does not influence the system's internal dynamics. Crucially, the dynamical invariant for the driven system is identified as $\hat{I}(t) = \hat{T}^\dagger(t)\hat{D}^\dagger(\alpha)\hat{N}_{\mathrm{exc}}\hat{D}(\alpha)\hat{T}(t)$, where $\hat{N}_{\mathrm{exc}} = \hat{a}^\dagger\hat{a} + \hat{\sigma}_z/2$ is the conserved total excitation number of the undriven system [23]. The unitary transformations that define this invariant are precisely those used to map the original time-dependent Hamiltonian onto its stationary counterpart. This invariant-based approach has proven effective in describing a wide range of light-matter systems with non-stationary interactions and beam propagation phenomena [25–27].

The factorization in Eq. (4) provides a rigorous framework for evaluating system observables in the Heisenberg picture. By expressing the time-evolved operators in terms of the standard Jaynes-Cummings evolution, we obtain:

$$\hat{a}(t) = \hat{U}^\dagger_{\mathtt{DJCM}}(t)\hat{a}(t)\hat{U}_{\mathtt{DJCM}}(t) = e^{-\mathrm{i}\omega_0 t}\left(\hat{D}^\dagger(\alpha)\hat{a}_{\mathtt{JCM}}(t)\hat{D}(\alpha) - \alpha\right), \tag{5a}$$

$$\hat{\sigma}_-(t) = \hat{U}^\dagger_{\mathtt{DJCM}}(t)\hat{\sigma}_-(t)\hat{U}_{\mathtt{DJCM}}(t) = e^{-\mathrm{i}\omega_0 t}\hat{D}^\dagger(\alpha)\hat{\sigma}_-^{\mathtt{JCM}}(t)\hat{D}(\alpha), \tag{5b}$$

where $\hat{O}_{\mathtt{JCM}}(t) = \hat{U}^\dagger_{\mathtt{JCM}}(t)\,\hat{O}\,\hat{U}_{\mathtt{JCM}}(t)$ represents the time-evolved operator in the Jaynes-Cummings basis. This representation offers a significant computational advantage for calculating the two-time correlation functions required to determine the time-dependent physical spectrum [29].

 doi:10.20944/preprints202512.2252.v1

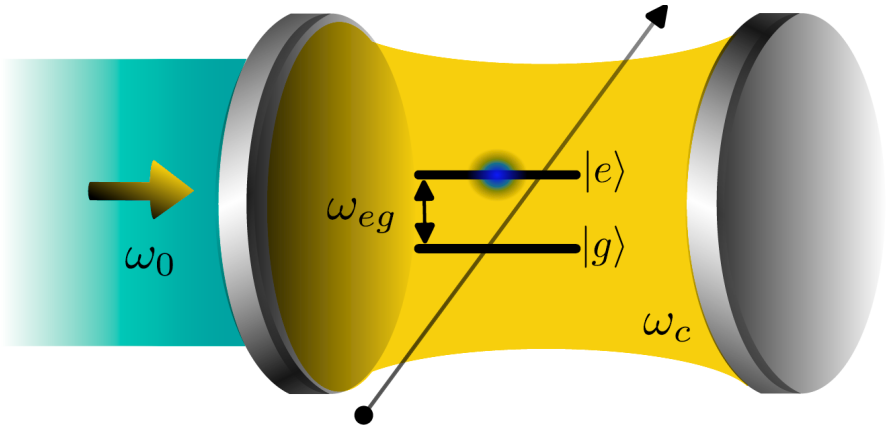

Figure 1. Schematic representation of the driven Jaynes-Cummings model. A two-level atom with transition frequency ω_{eg} is coupled to a single-mode cavity field of frequency ω_c. Both the atom and the cavity mode are simultaneously driven by an external classical field of frequency ω_0.

2.1. The Jaynes-Cummings Hamiltonian in the Block Diagonal Basis

To evaluate the two-time correlation functions, it is advantageous to exploit the symmetries and the diagonalization of the standard Jaynes-Cummings model. Since the Hamiltonian $\hat{H}_{\text{JCM}}$ commutes with the total excitation number operator $\hat{N}_{\text{exc}} = \hat{a}^\dagger\hat{a} + \hat{\sigma}_z/2$, the Hilbert space decomposes into an infinite set of invariant subspaces $\mathcal{H}_n$, each spanned by the basis states $\{|e,n\rangle, |g,n+1\rangle\}$. Within each n-th excitation subspace, the Hamiltonian is represented by the 2×2 matrix:

$$H^{(n)}_{\text{JCM}} = \begin{pmatrix} \Delta_c n + \frac{\Delta_{eg}}{2} & g\sqrt{n+1} \\ g\sqrt{n+1} & \Delta_c(n+1) - \frac{\Delta_{eg}}{2} \end{pmatrix}, \quad \text{with} \quad \begin{aligned} \Delta_c &= \omega_c - \omega_0, \\ \Delta_{eg} &= \omega_{eg} - \omega_0, \end{aligned} \tag{6}$$

where $g\sqrt{n+1}$ is the vacuum Rabi frequency characteristic of the n-th manifold. Diagonalizing this matrix yields the eigenenergies of the dressed states (polaritons):

$$\begin{aligned} \mathcal{E}^{(\pm)}_n &= \Delta_c\left(n+\frac{1}{2}\right) \pm \frac{1}{2}\sqrt{(\Delta_{eg}-\Delta_c)^2 + 4g^2(n+1)}, \\ &= \Delta_c\left(n+\frac{1}{2}\right) \pm \frac{1}{2}\sqrt{(\omega_{eg}-\omega_c)^2 + 4g^2(n+1)}, \end{aligned} \tag{7}$$

and eigenstates

$$|+,n\rangle = \cos\left(\frac{\theta_n}{2}\right)|e,n\rangle + \sin\left(\frac{\theta_n}{2}\right)|g,n+1\rangle, \tag{8a}$$

$$|-,n\rangle = \sin\left(\frac{\theta_n}{2}\right)|e,n\rangle - \cos\left(\frac{\theta_n}{2}\right)|g,n+1\rangle. \tag{8b}$$

Here, the mixing angle θ_n quantifies the degree of light-matter entanglement and is determined by the ratio of the coupling strength to the detuning: $\tan(\theta_n) = \frac{2g\sqrt{n+1}}{\omega_{eg}-\omega_c}$.

Eqs. (8a)–(8b) establish the representation of the propagator. The states $\{|\pm,n\rangle\}$ diagonalize $\hat{U}_{\text{JCM}}(t) = \exp(-i\hat{H}_{\text{JCM}}t)$. The operator consists of the sum of projectors onto the manifolds, weighted by phase factors:

$$\hat{U}_{\text{JCM}}(t) = e^{i\frac{\Delta_{eg}t}{2}}|g,0\rangle\langle g,0| + \sum_{n=0}^{\infty}\left[e^{-i\mathcal{E}^{(+)}_n t}|+,n\rangle\langle +,n| + e^{-i\mathcal{E}^{(-)}_n t}|-,n\rangle\langle -,n|\right]. \tag{9}$$

Eq. (9) provides the solution for the evolution in the manifold basis. Although the drive introduces the displacement $\hat{D}(\alpha)$ (where $\alpha = \zeta/g = /\xi/\Delta_c$) from Eqs. (5a)–(5b) and removes the diagonality of the propagator, the decomposition remains the foundation for the derivation of the dynamics. This

 doi:10.20944/preprints202512.2252.v1

representation enables the mapping of the state vector and the calculation of the correlation functions, which constitute the basis for the study of the spectrum.

3. The Time-Dependent Physical Spectrum

The time-dependent physical spectrum, defined by Eberly and Wódkiewicz [29], is given by the integral:

$$S(\Gamma,\omega;t) = 2\Gamma e^{-2\Gamma t}\int_0^t dt_1 \int_0^t dt_2\, e^{(\Gamma-i\omega)t_1} e^{(\Gamma+i\omega)t_2}\,\langle \hat{A}(t_1)\hat{B}(t_2)\rangle\,, \tag{10}$$

where $\langle \hat{A}(t_1)\hat{B}(t_2)\rangle$ is the two-time correlation function of system operators for an initial state $|\psi(0)\rangle$. Emission dynamics are determined by the spectral response of the atomic and electromagnetic field subsystems. The system is initialized in $|\psi(0)\rangle = |e,\beta\rangle$, representing an excited atom and a coherent field of amplitude β.

Utilizing the operator transformations in Eqs. (5a)–(5b), the dynamics are mapped into the standard Jaynes-Cummings frame. The correlation functions are thus expressed in terms of the effective coherent state $|\gamma\rangle = |\alpha+\beta\rangle$. The field and atomic correlation functions are:

$$\langle \hat{a}^\dagger(t_1)\hat{a}(t_2)\rangle = e^{i\omega_0(t_1-t_2)}\,\langle e,\gamma|\left[\hat{a}^\dagger_{\mathtt{JCM}}(t_1)\hat{a}_{\mathtt{JCM}}(t_2) - \alpha\left(\hat{a}^\dagger_{\mathtt{JCM}}(t_1)+\hat{a}_{\mathtt{JCM}}(t_2)\right)+\alpha^2\right]|e,\gamma\rangle\,, \tag{11}$$

where $\alpha = \zeta/g = \xi/\Delta_c$ links the driven Hamiltonian in (2) to the Jaynes-Cummings form in (3). The atomic correlation function is:

$$\langle \hat{\sigma}_+(t_1)\hat{\sigma}_-(t_2)\rangle = e^{i\omega_0(t_1-t_2)}\,\langle e,\gamma|\hat{\sigma}^{\mathtt{JCM}}_+(t_1)\hat{\sigma}^{\mathtt{JCM}}_-(t_2)|e,\gamma\rangle\,. \tag{12}$$

These expressions utilize the displacement operator property $\hat{D}(\alpha)\,|\beta\rangle = \hat{D}(\alpha)\hat{D}(\beta)\,|0\rangle = |\alpha+\beta\rangle$ with real amplitudes $\alpha,\beta\in\mathbb{R}$. This mapping determines the correlation functions for the effective state $|\gamma\rangle = |\alpha+\beta\rangle$, where β is the initial field amplitude and $\alpha = \zeta/g = \xi/\Delta_c$ links the driven Hamiltonian in (2) to the Jaynes-Cummings form in (3). Tuning the drive to cancel the initial field ($\gamma = -\beta$) recovers the vacuum Rabi splitting in the emission spectrum.

Although the preceding formalism applies to both the field and atomic subsystems, we focus our analysis on the atomic spectral response to clearly highlight the light-matter interaction signatures. Accordingly, the final analytical expression for the time-dependent atomic physical spectrum is (see Appendix A for the full derivation):

$$S_{\mathtt{atom}}(\Gamma,\omega;t) = 2\Gamma e^{-2\Gamma t}\left[S_{\mathrm{vac}}(t) + \sum_{n=1}^{\infty} S_n(t)\right]. \tag{13}$$

The vacuum contribution ($n=0$) results from decay into the ground state. The laboratory frequencies $\nu_0^{(\pm)} = \omega_0 + \mathcal{E}_0^{(\pm)} + \Delta_{eg}/2$ lead to:

$$S_{\mathrm{vac}}(t) = e^{-|\gamma|^2}\left|\cos^2\left(\frac{\theta_0}{2}\right)\mathcal{L}(\nu_0^{(+)}-\omega;t) + \sin^2\left(\frac{\theta_0}{2}\right)\mathcal{L}(\nu_0^{(-)}-\omega;t)\right|^2, \tag{14}$$

where

$$\mathcal{L}(\delta;t) = \frac{e^{(\Gamma+i\delta)t}-1}{\Gamma+i\delta}. \tag{15}$$

 doi:10.20944/preprints202512.2252.v1

The contribution from excited manifolds ($n \geq 1$) results from the four transition paths with $\nu_n^{(j,k)} = \omega_0 + \mathcal{E}_n^{(j)} - \mathcal{E}_{n-1}^{(k)}$:

$$\begin{aligned} S_n(t) = P_n \Bigg[& \sin^2\left(\frac{\theta_{n-1}}{2}\right) \left| \cos^2\left(\frac{\theta_n}{2}\right) \mathcal{L}\left(\nu_n^{(+,+)} - \omega; t\right) + \sin^2\left(\frac{\theta_n}{2}\right) \mathcal{L}\left(\nu_n^{(-,+)} - \omega; t\right) \right|^2 \\ & + \cos^2\left(\frac{\theta_{n-1}}{2}\right) \left| \cos^2\left(\frac{\theta_n}{2}\right) \mathcal{L}\left(\nu_n^{(+,-)} - \omega; t\right) + \sin^2\left(\frac{\theta_n}{2}\right) \mathcal{L}\left(\nu_n^{(-,-)} - \omega; t\right) \right|^2 \Bigg], \end{aligned} \tag{16}$$

where $P_n = e^{-|\gamma|^2} |\gamma|^{2n} / n!$, and

$$\begin{aligned} \sin^2\left(\frac{\theta_n}{2}\right) &= \frac{1}{2}\left(1 - \frac{\omega_{eg} - \omega_c}{\sqrt{(\omega_{eg} - \omega_c)^2 + 4g^2(n+1)}}\right), \\ \cos^2\left(\frac{\theta_n}{2}\right) &= \frac{1}{2}\left(1 + \frac{\omega_{eg} - \omega_c}{\sqrt{(\omega_{eg} - \omega_c)^2 + 4g^2(n+1)}}\right). \end{aligned} \tag{17}$$

The analytical results derived in Eq. (13) provide a comprehensive framework for characterizing the multi-manifold emission dynamics of the driven system, which we elucidate through the atomic physical spectra displayed in Figures 2 and 3. In Figure 2, we illustrate the progressive emergence of spectral resolution as a function of the interaction time t; at early stages ($\Gamma t \approx 1$, the spectrum is dominated by broad, overlapping profiles due to the Fourier-limited resolution of the Eberly–Wódkiewicz windowing, whereas in the asymptotic regime ($\Gamma t \gg 1$), transient frequency fluctuations are exponentially suppressed, revealing discrete resonances associated with transitions between polaritonic manifolds. A salient feature in this temporal evolution is the pronounced asymmetry in the spectral peak heights, which constitutes a fundamental signature of off-resonant coupling. For finite detuning ($\omega_{eg} \neq \omega_c$), the dressed states $\{|\pm, n\rangle\}$ acquire unequal atomic and photonic components—as governed by the mixing angles θ_n in Eq. (8a)—thereby favoring transition paths with higher atomic weighting. This imbalance reflects the structural properties of the light-matter entanglement, where the emission process preferentially tracks the atomic population distribution across the Jaynes-Cummings ladder.

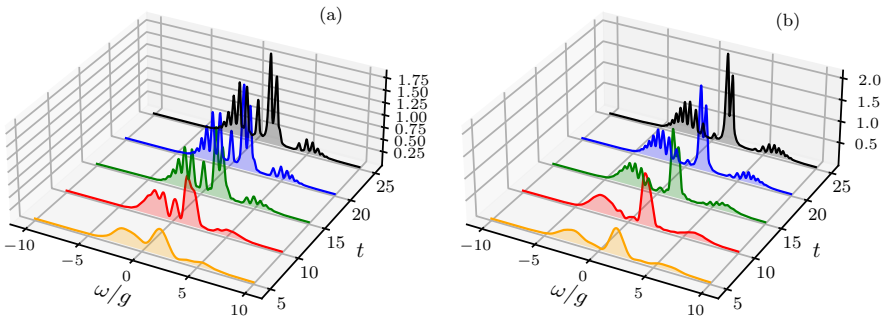

Figure 2. Temporal evolution of the atomic physical spectrum $S_{\mathtt{atom}}(\Gamma, \omega; t)$, highlighting the progressive emergence of dressed-state resonances across multiple interaction timescales. At incipient times, the spectral response is characterized by a broad, unresolved profile, a direct consequence of the Fourier-limited resolution intrinsic to the Eberly-Wódkiewicz windowing. As the interaction time increases ($t \gg \Gamma^{-1}$), the transient frequency fluctuations are exponentially suppressed, allowing the spectrum to resolve into a discrete set of sharp resonances associated with transitions between polaritonic manifolds in the Jaynes-Cummings ladder. The observable peak asymmetries and the underlying oscillatory modulations reflect the interplay between the off-resonant coupling and the coherent displacement induced by the external drive. Simulation parameters: $g = 1.0$, $\omega_0 = 1.95$, $\omega_{eg} = 1.00$, $\omega_c = 1.75$, $\beta = 3$, and $\Gamma = 0.1$. Panel (a) corresponds to a weak-driving scenario with $\xi = 0.3$ ($\alpha = \zeta/g = \xi/\Delta_c \approx -1.5$), while panel (b) illustrates the substantial spectral reshaping occurring in the high-driving regime with $\xi = 1.0$ ($\alpha \approx -5.0$).

 doi:10.20944/preprints202512.2252.v1

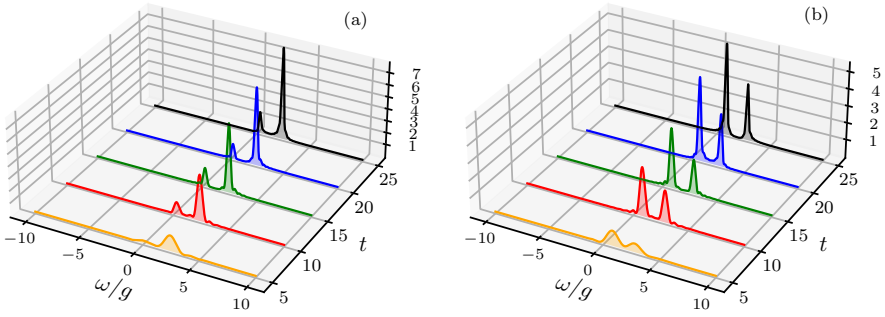

Figure 3. Atomic physical spectrum $S_{\mathtt{atom}}(\Gamma, \omega; t)$ as a function of frequency ω at various interaction times, demonstrating the deterministic recovery of the fundamental vacuum Rabi splitting. The results illustrate that the external driving mechanism facilitates the exact coherent cancellation of the initial cavity field when the effective coherence parameter vanishes ($\gamma = 0$ for $\beta = -\alpha$). Case (a) corresponds to a cavity frequency $\omega_c = 1.0$ (leading to an atomic drive amplitude $\alpha = \zeta/g = \xi/\Delta_c \approx -1.05$), while case (b) examines the regime with $\omega_c = 2.0$ ($\alpha = \zeta/g = \xi/\Delta_c \approx 19.0$). In both scenarios, the suppression of higher-order Mollow-like sidebands reveals the underlying vacuum Rabi doublet, highlighting a controllable transition from a driven many-photon regime to a vacuum-mediated light-matter interaction. Simulation parameters: $g = 1.0$, $\omega_0 = 1.95$, $\omega_{eg} = 1.75$, $\xi = 1.0$, and $\Gamma = 0.1$.

Beyond these temporal dynamics, Figure 3 shows the recovery of the vacuum limit through the cancellation of the field amplitude. When the drive satisfies the condition $\beta = -\alpha$, with $\alpha = \zeta/g = \xi/\Delta_c$, the effective coherence parameter vanishes ($\gamma = 0$). This condition results from the destructive interference between the external drive and the initial cavity field at the atom's location, formulated through the unitary displacement $D(\alpha)$ in the rotating frame. This cancellation maps the driven two-time correlation function in Eq. (12) to the undriven vacuum case and restricts the system evolution to the Jaynes-Cummings dynamics in the displaced basis. Within this framework, the time-dependent dynamical invariant recovers its undriven algebraic structure, formulated explicitly as

$$\hat{I}(t) = \hat{T}^{\dagger}(t)\hat{D}^{\dagger}(\alpha)\left(\hat{a}^{\dagger}\hat{a} + \frac{\hat{\sigma}_z}{2}\right)\hat{D}(\alpha)\hat{T}(t), \tag{18}$$

while the effective Hamiltonian becomes time-independent in the rotating frame. The Poissonian weights P_n in Eq. (13) collapse to the Kronecker delta $\delta_{n,0}$, which reduces the system response from a weighted sum over the infinite ladder of dressed-state manifolds to a single-excitation subspace. The weights of all manifolds $n \geq 1$, which scale as $|\gamma|^{2n}$ according to the Poisson distribution, are zero, and the interaction is confined to transitions between the polaritonic doublet $\{|+,0\rangle, |-,0\rangle\}$ and the absolute ground state $|g,0\rangle$ in the displaced frame. The spectral response is defined by these transitions, which produce a doublet at the laboratory frequencies $\omega = \omega_0 \pm \sqrt{\Delta^2/4 + g^2} + \Delta_{eg}/2$ (with $\Delta = \omega_{eg} - \omega_c$). For the resonant regime ($\omega_{eg} = \omega_c$), the peak separation remains fixed at the vacuum Rabi frequency $\Omega_0 = 2g$. The intensities of these resonances are determined by the mixing angle θ_0, where the detuning Δ introduces a height asymmetry corresponding to the atomic population weighting of the dressed states. Specifically, the spectral intensities are defined by the analytical weights $\mathcal{W}_0^{(\pm)} = \frac{1}{4}(1 \pm \Delta/\Omega_0)^2$ (with $\Delta = \omega_{eg} - \omega_c$), which dictate the emission rate into the zero-photon sector from the upper and lower polaritons, respectively. These weights arise from the projection of the atomic transition operator onto the polaritonic eigenbasis of the dynamical invariant $\hat{I}(t)$ and reflect the degree of light-matter mixing. In this limit, the multi-manifold interference that generates the sidebands in the $\gamma \neq 0$ regime is suppressed because the field enters the dynamics through the vacuum state fluctuations. This mechanism suppresses the Mollow-like structures and isolates the vacuum-field coupling signatures at the single-photon level. As the interaction time t increases in this regime, the detector bandwidth Γ resolves the underlying energy levels of the Jaynes-Cummings

 doi:10.20944/preprints202512.2252.v1

ladder, leading to a reduction in the Lorentzian linewidths. The drive acts as a control parameter to cancel the mean field amplitude and resolve the vacuum-mediated splitting in an externally driven system where the driving effect is nullified in the rotating frame defined by the invariant framework of transformations. This allows for the investigation of fundamental vacuum effects in the presence of strong external fields through the exact coherent compensation of the field-atom driving.

3.1. Steady-State Atomic Physical Spectrum

The spectral resolution of the Eberly–Wódkiewicz windowing is fundamentally constrained by the interaction time t. The transient dynamics shown in Figure 2 resolve into a stationary structure in the asymptotic limit $\Gamma t \gg 1$. To characterize the steady-state emission, we evaluate the limit of Eq. (13) as $t \to \infty$. Utilizing the definition of the windowing function $\mathcal{L}(\delta; t)$ in Eq. (13) (see Eq. (15)), the relevant term for the spectral intensity scales as

$$2\Gamma e^{-2\Gamma t}|\mathcal{L}(\delta;t)|^2 = \frac{2\Gamma\left(1 - 2e^{-\Gamma t}\cos(\delta t) + e^{-2\Gamma t}\right)}{\Gamma^2 + \delta^2}. \tag{19}$$

In the limit where $t \to \infty$, the exponential terms vanish, and the normalized windowing function converges to a Lorentzian profile

$$\lim_{t\to\infty} 2\Gamma e^{-2\Gamma t}|\mathcal{L}(\delta;t)|^2 = \frac{2\Gamma}{\Gamma^2 + \delta^2}, \tag{20}$$

with a full-width at half-maximum determined by the detector bandwidth 2Γ. While the time-dependent spectrum in Eqs. (14) and (16) involves the absolute square of a sum of windowing functions, the stationary representation relies on the resolved peak approximation. When the separation between polaritonic resonances $\Delta\nu$ satisfies $\Delta\nu \gg \Gamma$, the spectral overlap between distinct Lorentzian profiles is negligible. Under these conditions, the cross-interference terms in $|\sum_j c_j \mathcal{L}_j|^2$ vanish, and the steady-state atomic physical spectrum reduces to a weighted sum of independent Lorentzian peaks:

$$\begin{aligned} S^{\infty}_{\mathtt{atom}}(\Gamma,\omega) = 2\Gamma e^{-|\gamma|^2}&\left[\mathcal{W}_0^{(+)}\frac{1}{\Gamma^2 + (\nu_0^{(+)} - \omega)^2} + \mathcal{W}_0^{(-)}\frac{1}{\Gamma^2 + (\nu_0^{(-)} - \omega)^2}\right] \\ &+ 2\Gamma\sum_{n=1}^{\infty} P_n \sum_{j,k\in\{+,-\}} \mathcal{W}_n^{(j,k)}\frac{1}{\Gamma^2 + (\nu_n^{(j,k)} - \omega)^2}, \end{aligned} \tag{21}$$

where the spectral weights $\mathcal{W}_0^{(\pm)}$ and $\mathcal{W}_n^{(j,k)}$ absorb the squared amplitudes:

$$\begin{aligned} \mathcal{W}_0^{(\pm)} &= \frac{1}{4}\left(1 \pm \frac{\Delta}{\Omega_0}\right)^2, \\ \mathcal{W}_n^{(j,\pm)} &= \frac{1}{8}\left(1 \mp \frac{\Delta}{\Omega_{n-1}}\right)\left(1 \pm \frac{\Delta\delta_{j,+} - \Delta\delta_{j,-}}{\Omega_n}\right)^2, \end{aligned} \tag{22}$$

with $\Delta = \omega_{eg} - \omega_c$ and $\Omega_n = \sqrt{\Delta^2 + 4g^2(n+1)}$. where the weights P_n represent the Poissonian distribution of excitation manifolds. This stationary representation highlights that the multi-peak structure observed in Figure 2 remains robust in the steady state, where the detector resolution Γ acts as the effective linewidth of the polaritonic resonances. In the vacuum limit ($\beta = -\alpha$), the sum in Eq. (21) collapses to the vacuum Rabi doublet, where the intensities reflect the degree of light-matter mixing at the single-excitation level.

4. Conclusions

In this work, we presented a complete analytical characterization of the time-dependent physical spectrum for the driven Jaynes-Cummings model. Our approach, grounded in the invariant

 doi:10.20944/preprints202512.2252.v1

framework [23], allowed for an exact algebraic treatment of the driven dynamics by mapping the time-dependent Hamiltonian onto a stationary, block-diagonal form. This methodology provided closed-form expressions for the atomic and field correlation functions, enabling the evaluation of the Eberly–Wódkiewicz spectrum [29] across all interaction time scales.

A fundamental insight gained from this analysis is the interpretation of the external drive as a coherent field displacement $\hat{D}(\alpha)$, which reshapes the photon-number distribution and uniquely modifies the spectral weights of the dressed-state ladder. We demonstrated that for resonant driving conditions ($\beta = -\alpha$), the mean-field fluctuations are coherently nullified, effectively mapping the system dynamics onto the undriven vacuum limit. This mechanism provides a transparent tool for isolating vacuum-field signatures in the presence of strong external fields, where the emission spectrum collapses to a symmetric vacuum Rabi doublet.

In the asymptotic interaction limit ($\Gamma t \gg 1$), we derived the steady-state atomic spectrum as a weighted sum of Lorentzian peaks. By invoking the resolved peak approximation—where the polaritonic separation exceeds the detector bandwidth—we established a rigorous justification for neglecting cross-interference terms between distinct resonances. The resulting representation highlights that the stationary asymmetry in peak heights is a structural property of the light-matter entanglement, determined by the algebraic weights $\mathcal{W}_n^{(j,k)}$ that quantify atomic population weighting within each excitation manifold.

Beyond its theoretical implications, our formulation offers a versatile platform for exploring time-resolved spectral control in modern cavity QED and circuit QED architectures [3,4]. The connection between coherent-field cancellation and the suppression of multi-manifold interference suggests potential applications in quantum state engineering and recently proposed concepts such as quantum catalysis [33], where light-matter interactions mediate the redistribution of quantum fluctuations. Future extensions to driven-dissipative scenarios and the incorporation of squeezed or non-classical initial states will further broaden the applicability of the invariant-based spectral analysis presented here.

Author Contributions: All authors contributed equally to each of the requirements necessary for the elaboration of this manuscript. All authors have read and agreed to the published version of the manuscript.

Funding: This research received no external funding.

Data Availability Statement: No new data were created or analyzed in this study.

Acknowledgments: L.M.D. thanks the Secretariat of Science, Humanities, Technology and Innovation (SECIHTI) for the doctoral scholarship.

Conflicts of Interest: The authors declare no conflict of interest.

Appendix A. Derivation of the Time-Dependent Physical Spectrum

In this appendix, we outline the exact derivation of the time-dependent atomic physical spectrum. The starting point is the two-time correlation function in the Heisenberg picture, $\langle \hat{\sigma}_+(t_1)\hat{\sigma}_-(t_2)\rangle = e^{i\omega_0(t_1-t_2)}\langle \Phi(t_1)|\Phi(t_2)\rangle$, where we define the atomic source state vector as:

$$|\Phi(t)\rangle = \hat{U}^\dagger_{\mathrm{JCM}}(t)\hat{\sigma}_-\hat{U}_{\mathrm{JCM}}(t)\,|e,\gamma\rangle\,. \tag{A1}$$

To evaluate this vector exactly, we expand the initial effective state $|e,\gamma\rangle = \sum_{n=0}^{\infty} C_n\,|e,n\rangle$ (with $C_n = e^{-|\gamma|^2/2}\gamma^n/\sqrt{n!}$) in terms of the dressed eigenstates $\{|+,n\rangle\,,|-,n\rangle\}$ of each manifold n. Utilizing the mapping rules $\hat{\sigma}_-\,|+,n\rangle = c_n\,|g,n\rangle$ and $\hat{\sigma}_-\,|-,n\rangle = s_n\,|g,n\rangle$, where $c_n = \cos(\theta_n/2)$ and $s_n = \sin(\theta_n/2)$, the forward and backward time evolution yields the explicit form:

$$|\Phi(t)\rangle = C_0 f_0(t) e^{i\frac{\Delta_{eg}}{2}t}\,|g,0\rangle + \sum_{n=1}^{\infty} C_n f_n(t)\left[s_{n-1}e^{i\mathcal{E}^{(+)}_{n-1}t}\,|+,n-1\rangle - c_{n-1}e^{i\mathcal{E}^{(-)}_{n-1}t}\,|-,n-1\rangle\right], \tag{A2}$$

 doi:10.20944/preprints202512.2252.v1

with the dynamical amplitudes defined as $f_n(t) = c_n^2 e^{-i\mathcal{E}_n^{(+)}t} + s_n^2 e^{-i\mathcal{E}_n^{(-)}t}$. The orthogonality of the dressed-state manifolds ensures that the inner product $\langle\Phi(t_1)|\Phi(t_2)\rangle$ collapses into a sum over independent manifolds $P_n = |C_n|^2$. By substituting the laboratory transition frequencies $\nu_n^{(j,k)} = \omega_0 + \mathcal{E}_n^{(j)} - \mathcal{E}_{n-1}^{(k)}$, the correlation function becomes a superposition of oscillating terms:

$$G_{\mathtt{atom}}(t_1,t_2) = P_0 \sum_{j\in\{+,-\}} \mathcal{W}_0^{(j)} e^{i\nu_0^{(j)}(t_1-t_2)} + \sum_{n=1}^{\infty} P_n \sum_{j,k\in\{+,-\}} \mathcal{W}_n^{(j,k)} e^{i\nu_n^{(j,k)}(t_1-t_2)}. \tag{A3}$$

The physical spectrum $S(\Gamma,\omega;t)$ is then obtained by inserting $G_{\mathtt{atom}}$ into the Eberly-Wódkiewicz integral in Eq. (10). Because each frequency component $\nu_n^{(j,k)}$ factorizes the double time integral into the product $|\mathcal{L}(\omega-\nu_n^{(j,k)};t)|^2$, the final spectrum resolves into the weighted sum provided in Eq. (13).

The spectral weights $\mathcal{W}_n^{(j,k)}$ quantify the atomic transition probabilities between the dressed-state ladders. These weights emerge from the squared amplitudes of the source state vector in Eq. (A2). For the vacuum contribution ($n = 0$), the transition occurs from the excited state $|e,0\rangle$ to the absolute ground state $|g,0\rangle$, mediated by the two polariton branches $|\pm,0\rangle$. The corresponding weights are:

$$\mathcal{W}_0^{(\pm)} = |c_0^2 \pm s_0^2|^2 = \frac{1}{4}\left(1 \pm \frac{\Delta}{\Omega_0}\right)^2, \tag{A4}$$

where $\Omega_0 = \sqrt{\Delta^2 + 4g^2}$ is the vacuum Rabi frequency and $\Delta = \omega_{eg} - \omega_c$ is the atom-cavity detuning. These weights describe the asymmetry of the vacuum Rabi doublet: at resonance ($\Delta = 0$), both peaks have equal intensity ($\mathcal{W}_0^{(+)} = \mathcal{W}_0^{(-)} = 1/4$), while off-resonance, one branch dominates over the other.

For the excited manifolds ($n \geq 1$), the atomic lowering operator induces transitions from manifold n to manifold $n-1$. Each transition involves four possible pathways, corresponding to the initial and final polariton indices $(j,k) \in \{+,-\} \times \{+,-\}$. The weights are:

$$\mathcal{W}_n^{(j,k)} = \frac{1}{8}\left(1 - k\frac{\Delta}{\Omega_{n-1}}\right)\left(1 + j\frac{\Delta}{\Omega_n}\right)^2, \tag{A5}$$

where $\Omega_n = \sqrt{\Delta^2 + 4g^2(n+1)}$ is the generalized Rabi frequency for the n-th manifold. The first factor, $(1 - k\Delta/\Omega_{n-1})/2$, represents the atomic character of the initial polariton state in manifold $n-1$, while the second factor, $(1 + j\Delta/\Omega_n)^2/4$, encodes the squared transition amplitude from manifold n. This factorization reflects the selection rules of the atomic dipole operator in the dressed basis.

The detuning-dependent structure of these weights is responsible for the spectral asymmetries observed in Figures 2 and 3. Specifically, when $\Delta > 0$ (atom blue-detuned from the cavity), the upper polariton branch ($j = +$) acquires a larger atomic component, enhancing the emission probability for transitions involving this state. Conversely, for $\Delta < 0$, the lower branch ($j = -$) dominates. This asymmetry is a fundamental signature of the light-matter hybridization and is directly encoded in the algebraic form of $\mathcal{W}_n^{(j,k)}$.

References

1. Jaynes, E.T.; Cummings, F.W. Comparison of quantum and semiclassical radiation theories with application to the beam maser. *Proc. IEEE* **1963**, *51*, 89–109. https://doi.org/10.1109/PROC.1963.1664.
2. Shore, B.W.; Knight, P.L. The Jaynes–Cummings model. *J. Mod. Opt.* **1993**, *40*, 1195–1238. https://doi.org/10.1080/09500349314551321.
3. Wallraff, A.; Schuster, D.I.; Blais, A.; Frunzio, L.; Huang, R.S.; Majer, J.; Kumar, S.; Girvin, S.M.; Schoelkopf, R.J. Strong coupling of a single photon to a superconducting qubit using circuit quantum electrodynamics. *Nature* **2004**, *431*, 162–167. https://doi.org/10.1038/nature02851.
4. Fink, J.M.; Göppl, M.; Baur, M.; Bianchetti, R.; Leek, P.J.; Blais, A.; Wallraff, A. Climbing the Jaynes–Cummings ladder and observing its nonlinearity in a cavity QED system. *Nature* **2008**, *454*, 315–318. https://doi.org/10.1038/nature07112.

 doi:10.20944/preprints202512.2252.v1

5. Eberly, J.H.; Narozhny, N.B.; Sanchez-Mondragon, J.J. Periodic Spontaneous Collapse and Revival in a Simple Quantum Model. *Phys. Rev. Lett.* **1980**, *44*, 1323–1326. https://doi.org/10.1103/PhysRevLett.44.1323.
6. Thompson, R.J.; Rempe, G.; Kimble, H.J. Observation of normal-mode splitting for an atom in an optical cavity. *Phys. Rev. Lett.* **1992**, *68*, 1132–1135. https://doi.org/10.1103/PhysRevLett.68.1132.
7. Sanchez-Mondragon, J.J.; Narozhny, N.B.; Eberly, J.H. Theory of spontaneous-emission line shape in an ideal cavity. *Phys. Rev. Lett.* **1983**, *51*, 550–553. https://doi.org/10.1103/PhysRevLett.51.550.
8. Zhu, Y.; Gauthier, D.J.; Morin, S.E.; Wu, Q.; Carmichael, H.J.; Mossberg, T.W. Vacuum Rabi splitting as a feature of linear-dispersion theory: Analysis and experimental observations. *Phys. Rev. Lett.* **1990**, *64*, 2499–2502. https://doi.org/10.1103/PhysRevLett.64.2499.
9. Yoshie, T.; Scherer, A.; Hendrickson, J.; Khitrova, G.; Gibbs, H.M.; Rupper, G.; Ell, C.; Shchekin, O.B.; Deppe, D.G. Vacuum Rabi splitting with a single quantum dot in a photonic crystal nanocavity. *Nature* **2004**, *432*, 200–203. https://doi.org/10.1038/nature03119.
10. Bužek, V.; Moya-Cessa, H.; Knight, P.L.; Phoenix, S.J.D. Schrödinger-cat states in the resonant Jaynes-Cummings model: Collapse and revival of oscillations of the photon-number distribution. *Phys. Rev. A* **1992**, *45*, 8190–8203. https://doi.org/10.1103/PhysRevA.45.8190.
11. Gea-Banacloche, J. Jaynes-Cummings model with quasiclassical fields: The effect of dissipation. *Phys. Rev. A* **1993**, *47*, 2221–2234. https://doi.org/10.1103/PhysRevA.47.2221.
12. Scala, M.; Militello, B.; Messina, A.; Piilo, J.; Maniscalco, S. Microscopic derivation of the Jaynes-Cummings model with cavity losses. *Phys. Rev. A* **2007**, *75*, 013811. https://doi.org/10.1103/PhysRevA.75.013811.
13. Sukumar, C.V.; Buck, B. Multi-phonon generalisation of the Jaynes–Cummings model. *Phys. Lett. A* **1981**, *83*, 211–213. https://doi.org/10.1016/0375-9601(81)90005-4.
14. Deppe, F.; Mariantoni, M.; Menzel, E.P.; Marx, A.; Saito, S.; Kakuyanagi, K.; Tanaka, H.; Meno, T.; Semba, K.; Takayanagi, H.; et al. Two-photon probe of the Jaynes–Cummings model and controlled symmetry breaking in circuit QED. *Nature Physics* **2008**, *4*, 686–691. https://doi.org/10.1038/nphys1016.
15. Ramos-Prieto, I.; Rodríguez-Lara, B.M.; Moya-Cessa, H.M. Engineering nonlinear coherent states as photon-added and photon-subtracted coherent states. *International Journal of Quantum Information* **2014**, *12*, 1560005. https://doi.org/10.1142/S0219749915600059.
16. Larson, J.; Mavrogordatos, T. *The Jaynes-Cummings Model and Its Descendants: Modern Research Directions*; IOP Publishing: Bristol, 2021. https://doi.org/10.1088/978-0-7503-6452-2.
17. Schmidt, S.; Koch, J. Circuit QED lattices: Towards quantum simulation with superconducting circuits. *Annalen der Physik* **2013**, *525*, 395–412. https://doi.org/10.1002/andp.201200261.
18. Anaya-Contreras, J.A.; Ramos-Prieto, I.; Zúñiga-Segundo, A.; Moya-Cessa, H.M. The anisotropic quantum Rabi model with diamagnetic term. *Frontiers in Physics* **2025**, *13*. https://doi.org/10.3389/fphy.2025.1568407.
19. Medina-Dozal, L.; Urzúa-Pineda, A.R.; Aranda-Lozano, D.; González-Gutiérrez, C.A.; Récamier, J.; Román-Ancheyta, R. Spectral response of a nonlinear Jaynes-Cummings model. *Phys. Rev. A* **2024**, *110*, 043703. https://doi.org/10.1103/PhysRevA.110.043703.
20. Alsing, P.; Guo, D.S.; Carmichael, H.J. Dynamic Stark effect for the Jaynes-Cummings system. *Phys. Rev. A* **1992**, *45*, 5135–5143. https://doi.org/10.1103/PhysRevA.45.5135.
21. Dutra, S.M.; Knight, P.L.; Moya-Cessa, H. Large-scale fluctuations in the driven Jaynes-Cummings model. *Phys. Rev. A* **1994**, *49*, 1993–1998. https://doi.org/10.1103/PhysRevA.49.1993.
22. Jyotsna, I.V.; Agarwal, G.S. The Jaynes-Cummings model with continuous external pumping. *Opt. Commun.* **1993**, *99*, 344–349. https://doi.org/10.1016/0030-4018(93)90341-2.
23. Bocanegra-Garay, I.A.; Hernández-Sánchez, L.; Ramos-Prieto, I.; Soto-Eguibar, F.; Moya-Cessa, H.M. Invariant approach to the driven Jaynes-Cummings model. *SciPost Phys.* **2024**, *16*, 007. https://doi.org/10.21468/SciPostPhys.16.1.007.
24. Lewis, H.R.; Riesenfeld, W.B. An Exact Quantum Theory of the Time-Dependent Harmonic Oscillator and of a Charged Particle in a Time-Dependent Electromagnetic Field. *J. Math. Phys.* **1969**, *10*, 1458–1473. https://doi.org/10.1063/1.1664991.
25. Ramos-Prieto, I.; Urzúa-Pineda, A.R.; Soto-Eguibar, F.; Moya-Cessa, H.M. KvN mechanics approach to the time-dependent frequency harmonic oscillator. *Sci. Rep.* **2018**, *8*, 8401. https://doi.org/10.1038/s41598-018-26759-w.
26. Ramos-Prieto, I.; Román-Ancheyta, R.; Soto-Eguibar, F.; Récamier, J.; Moya-Cessa, H.M. Temporal factorization of a nonstationary electromagnetic cavity field. *Phys. Rev. A* **2023**, *108*, 033720. https://doi.org/10.1103/PhysRevA.108.033720.

 doi:10.20944/preprints202512.2252.v1

27. Huerta-Sandoval, M.; Uriostegui, K.; Ramos-Prieto, I.; Soto-Eguibar, F.; Moya-Cessa, H. Unitary transformation approach to the paraxial wave equation, 2025, [arXiv:physics.optics/2510.00277].
28. Castro-Beltrán, H.M.; Román-Ancheyta, R.; Gutiérrez, L. Phase-dependent fluctuations of intermittent resonance fluorescence. *Phys. Rev. A* **2016**, *93*, 033801. https://doi.org/10.1103/PhysRevA.93.033801.
29. Eberly, J.H.; Wódkiewicz, K. The time-dependent physical spectrum of light. *J. Opt. Soc. Am.* **1977**, *67*, 1252–1261. https://doi.org/10.1364/JOSA.67.001252.
30. Diels, J.C.; Rudolph, W. *Ultrashort Laser Pulse Phenomena: Fundamentals, Techniques, and Applications on a Femtosecond Time Scale*, 2nd ed.; Academic Press: Amsterdam, 2006.
31. Carmichael, H.J. *Statistical Methods in Quantum Optics 1: Master Equations and Fokker-Planck Equations*; Springer: Berlin Heidelberg, 1999. https://doi.org/10.1007/978-3-662-03875-8.
32. Glauber, R.J. Coherent and Incoherent States of the Radiation Field. *Phys. Rev.* **1963**, *131*, 2766–2788. https://doi.org/10.1103/PhysRev.131.2766.
33. de Oliveira Junior, A.; Perarnau-Llobet, M.; Brunner, N.; Lipka-Bartosik, P. Quantum catalysis in cavity QED. *Phys. Rev. Research* **2024**, *6*, 023127. https://doi.org/10.1103/PhysRevResearch.6.023127.